Modulation of Self-Assembly Enhances the Catalytic Activity of Iron Porphyrin for CO_2 Reduction

Masahiro Tasaki, Yuki Okabe, Hikaru Iwami, Chiharu Akatsuka, Kento Kosugi, Kohei Negita, Sinpei Kusaka, Ryotaro Matsuda, Mio Kondo, and Shigeyuki Masaoka**

Dedicated to the memory of Prof. Dr. Jean-Michel Savéant, who made a great contribution to this field

Electrochemical reduction of CO_2 in aqueous media is an important reaction to produce value-added carbon products in an environmentally and economically friendly manner. Various molecule-based catalytic systems for the reaction have been reported thus far. The key features of state-of-the-art catalytic systems in this field can be summarized as follows: 1) an iron-porphyrin-based scaffold as a catalytic center, 2) a dinuclear active center for the efficient activation of a CO_2 molecule, and 3) a hydrophobic channel for the accumulation of CO_2. This article reports a novel approach to construct a catalytic system for CO_2 reduction with the aforementioned three key substructures. The self-assembly of a newly designed iron-porphyrin complex bearing bulky substituents with noncovalent interaction ability forms a highly ordered crystalline solid with adjacent catalytically active sites and hydrophobic pores. The obtained crystalline solid serves as an electrocatalyst for CO_2 reduction in aqueous media. Note that a relevant iron-porphyrin complex without bulky substituents cannot form a porous structure with adjacent active sites, and the catalytic performance of the crystals of this relevant iron-porphyrin complex is substantially lower than that of the newly developed catalytic system. The present study provides a novel strategy for constructing porous crystalline solids for small-molecule conversions.

1. Introduction

Due to the increased demand for a sustainable society, the production of clean chemical fuels from abundant resources has been highly sought after in recent years.[1] In this context, the CO_2 reduction reaction underpins broad interest because this technology can produce value-added carbon products and counteract CO_2 emissions.[2] In particular, CO_2 reduction in aqueous media is an advantageous approach because water is an inexpensive, abundant, and environmentally benign solvent that facilitates proton and electron transfer, which is required to drive catalysis. Based on this background, vast efforts have been devoted to the development of molecule-based catalysts for CO_2 reduction.[3,4] The most significant advantage of molecule-based catalysts is their high tunability for catalytic activity based on the precise modification of molecular structures. From the excellent examples of state-of-the-art molecule-based catalysts for CO_2 reduction, we can extract the following important features to achieve efficient catalysis (**Scheme 1**a). First, iron-porphyrin complexes[4c,d,h,5] are a promising catalytic platform for CO_2 reduction because the complexes are based on earth-abundant metal ions and show extremely high catalytic activity. Additionally, their ease of structural modification enables fine-tuning of the activity.[4c,d,h,5,6] Second, dinuclear complexes with closely positioned metal centers can accelerate catalysis.[3k,4i,j] This fact indicates that the presence of adjacent catalytic active

M. Tasaki, Dr. Y. Okabe, H. Iwami
Department of Life and Coordination-Complex Molecular Science
Institute for Molecular Science (IMS)
5-1 Higashiyama, Myodaiji, Okazaki, Aichi 444-8787, Japan

M. Tasaki, Dr. Y. Okabe, H. Iwami
Department of Structural Molecular Science
SOKENDAI (The Graduate University for Advanced Studies)
Shonan Village, Hayama, Kanagawa 240-0193, Japan

H. Iwami, C. Akatsuka, K. Kosugi, Prof. M. Kondo, Prof. S. Masaoka
Division of Applied Chemistry
Graduate School of Engineering
Osaka University
2-1 Yamadaoka, Suita, Osaka 565-0871, Japan
E-mail: mio@chem.eng.osaka-u.ac.jp; masaoka@chem.eng.osaka-u.ac.jp

K. Negita, Dr. S. Kusaka, Prof. R. Matsuda
Department of Chemistry and Biotechnology
School of Engineering
Nagoya University
Chikusa-ku, Nagoya 464-8603, Japan

Prof. M. Kondo
JST
PRESTO
4-1-8 Honcho, Kawaguchi 332-0012, Japan

Prof. M. Kondo, Prof. S. Masaoka
Innovative Catalysis Science Division
Institute for Open and Transdisciplinary Research Initiatives (ICS-OTRI)
Osaka University
Suita, Osaka 565-0871, Japan

The ORCID identification number(s) for the author(s) of this article can be found under https://doi.org/10.1002/smll.202006150.

DOI: 10.1002/smll.202006150

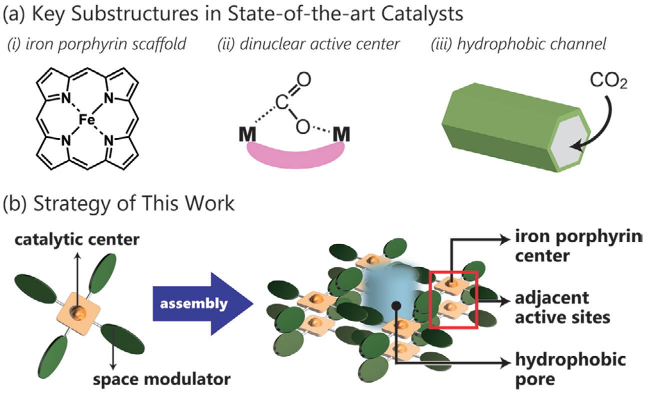

Scheme 1. Schematic illustration of a) three key substructures for CO reduction in state-of-the-art catalysts and b) the strategy of this work.

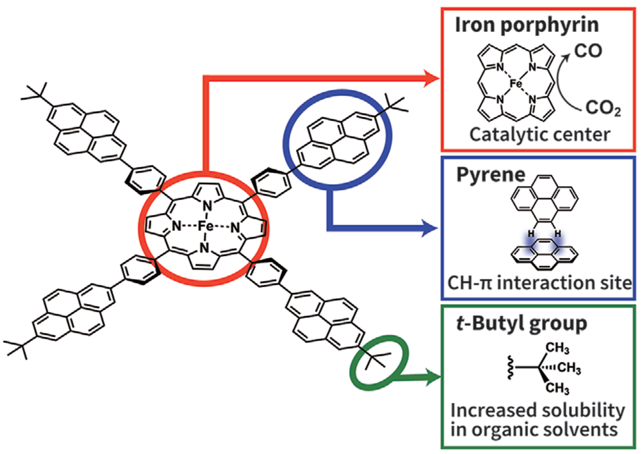

Scheme 2. Schematic illustration of a novel iron-porphyrin complex developed in this study.

centers is important to efficiently activate the substrate molecule CO_2. Third, the use of metal–organic frameworks (MOFs), covalent organic frameworks (COFs), and hydrogen-bonded frameworks (HOFs) is an intriguing approach.[3g,j,4e,f,j,m,n,7] These molecule-based crystalline porous materials can possess hydrophobic pores, which are suitable for the selective accumulation of CO_2 even in aqueous media. Such features of the MOFs and COFs enable catalysis in aqueous media by preventing kinetically favored side reaction, the reduction of water. Therefore, a molecule-based catalyst that exhibits the aforementioned three key features is expected to be an excellent candidate. However, to our knowledge, the literature contains no reports on such catalytic systems, and thus, the establishment of a strategy to obtain materials with three key features is highly desired.

In this contribution, we report an iron-porphyrin-based crystalline solid with adjacent catalytically active sites and hydrophobic pores. Our strategy here is to introduce bulky peripheral substituents with intermolecular interaction ability ("space modulators") to the iron-porphyrin unit (Scheme 1b). Intermolecular interactions between space modulators enable the assembly of catalyst molecules in an ordered fashion. As a result, catalytic centers can arrange with the appropriate distance for the activation of CO_2 molecules. The assembly also provides well-ordered hydrophobic pores for CO_2 accumulation, which is similar to the case of conventional MOFs, COFs, and HOFs. Another inherent feature of our strategy is that the porous crystalline solid can easily be prepared by the simple recrystallization technique. Notably, the obtained porous solid can be disassembled to a discrete state by using the appropriate solvent, which allows us to disclose the effect of the porous crystalline structure on the catalytic activity. Described here is the synthesis, characterization, and electrocatalytic activity for CO_2 reduction of the novel porous crystalline solid.

2. Results and Discussion

A key to success for obtaining the porous crystalline catalyst is to use a molecular module that has a catalytic center moiety with peripheral intermolecular interaction sites. **Scheme 2** illustrates the design of the molecular module developed in this study (5,10,15,20-tetrakis(4-(7-*tert*-butyl)pyren-2-yl)phenyl)porphyrinato iron(III) chloride, **Fe-BPPy**). The characteristics of this module can be summarized as follows. First, **Fe-BPPy** contains an iron-porphyrin moiety that can serve as an excellent catalyst for CO_2 reduction reactions and thus can be regarded as a suitable motif for catalytic centers. Note also that the fourfold (D_{4h}) symmetry of the iron-porphyrin unit is expected to be advantageous for the construction of a highly ordered framework structure. Second, **Fe-BPPy** possesses four bulky pyrenylphenyl moieties as space modulators. Pyrene derivatives are known to exhibit face-to-edge (CH–π) interactions between molecules and easily form the assembled structure.[8] The bulkiness of pyrene moieties are expected to prevent the π–π stacking of the porphyrin moieties and control the distance between iron centers. Third, *tert*-butyl groups are introduced at the 7-positions of the pyrene moieties. These groups are expected to enhance the solubility of the molecule, which is advantageous to control the assembly/disassembly process of the molecule.

The syntheses of the molecular module **Fe-BPPy** were performed according to the procedure shown in Scheme S1 in the Supporting Information. Initially, the Suzuki–Miyaura coupling of 2-bromo-7-*tert*-butylpyrene was reacted with 4-formylphenylboronic acid to afford 4-(7-(*tert*-butyl)pyrene-2-yl) benzaldehyde in 67% yield. The obtained aldehyde derivative was then reacted with pyrrole in the presence of trifluoroacetic acid (TFA) in CH_2Cl_2 at room temperature to provide a macrocyclic structure. Subsequently, 2,3-dichloro-5,6-dicyano-*p*-benzoquinone (DDQ) was added to the reaction mixture to oxidize the porphyrinogen, and the free base porphyrin (5,10,15,20-tetrakis(4-(7-*tert*-butyl)pyren-2-yl)phenyl)porphyrin, **H-BPPy**) was obtained in 24% yield. The **H-BPPy** was characterized by elemental analysis and ^{1}H NMR spectroscopy. The metal insertion reaction to the free base porphyrin, **H-BPPy**, was performed by heating the mixture of **H-BPPy** and iron(II) chloride tetrahydrate as a metal source under reflux conditions in *o*-dichlorobenzene (*o*-DCB) for 1.5 h. After the reaction, methanol was added to the reaction mixture to form a precipitate. The precipitate was collected by filtration, and the targeted compound, **Fe-BPPy**, was obtained with 80% yield. **Fe-BPPy** was characterized by elemental analysis and UV–vis absorption spectroscopy.

UV–vis absorption spectra of **H-BPPy** and **Fe-BPPy** were measured in *o*-DCB, and the results are shown in Figures S3 and S4 in the Supporting Information. The spectrum of the iron-porphyrin complex without pyrene moieties, 5,10,15,20-tetrakis(phenyl)porphyrinato iron(III) chloride (**Fe-TPP**), is also displayed in Figure S5 in the Supporting Information. In the spectrum of **H-BPPy**, sharp bands that are assignable to pyrene moieties[9] were observed in the UV region (λ_{max} = 314, 328, and 344 nm; Table S1, Supporting Information). In addition, a strong absorption band, the so-called Soret band, and four weaker bands, the so-called Q-bands, were observed at 430 nm and at 521, 558, 596, and 652 nm, respectively. These absorption bands in the visible region are characteristic of porphyrin derivatives.[10] The **Fe-BPPy** exhibited bands attributed to the pyrene moieties at 314, 329, and 344 nm and a Soret band associated with the porphyrin moiety at 428 nm. The position of these bands is similar to that of **H-BPPy**. In contrast, **Fe-BPPy** exhibited a smaller number of Q-bands (λ_{max} = 513, 557, and 695 nm) than **H-BPPy**. This is due to the degeneration of the highest occupied molecular orbital (HOMO) and the HOMO-1 upon the generation of more symmetric structures via metalation.[11] This observation supports that an iron ion is inserted into the porphyrin ring of **Fe-BPPy**. Notably, the positions of the Soret band and Q-bands are almost identical between **Fe-BPPy** and **Fe-TPP** (Soret band: λ_{max} = 420 nm, Q-bands: λ_{max} = 510, 556, and 691 nm; Table S1, Supporting Information), which suggests that the electronic structure of the porphyrin unit in **Fe-BPPy** is analogous to that of **Fe-TPP**.

Subsequently, the electrochemical properties of the porphyrins were investigated. **Figure 1**a shows cyclic voltammograms (CVs) of the porphyrins in 0.1 M tetra-*n*-butyl ammonium perchlorate (TBAP)/*o*-DCB under Ar atmosphere. **H-BPPy** exhibited two reversible redox waves at –1.72 and –2.00 V (vs ferrocene/ferrocenium (Fc/Fc$^+$); Figure 1a, black line), and these waves are assigned to the reduction processes of the porphyrin moiety.[12] In the CV of **Fe-BPPy**, three reversible redox waves were observed at –0.83, –1.58, and –2.17 V (Figure 1a, red line; Table S2, Supporting Information), and these peaks are putatively assigned to Fe(III)/Fe(II), Fe(II)/Fe(I), and Fe(I)/Fe(0) redox couples according to a previous report.[13] For the CV of **Fe-TPP**, three redox peaks assignable to the reduction processes of the iron ion were observed at –0.84, –1.61, and –2.23 V (Figure 1a, blue; Table S2, Supporting Information), and the redox potentials of **Fe-TPP** are quite similar to those of **Fe-BPPy**. It should be also noted that the redox potentials **Fe-TPP** in 0.1 M TBAP/*o*-DCB are almost identical to the reported values.[6c] The results demonstrate that the effect of pyrene moieties on the electronic structure of the porphyrin moiety is almost negligible and is consistent with the results of UV–vis absorption spectroscopy (vide supra). We also performed electrochemical measurements of **Fe-BPPy** under a CO_2 atmosphere to investigate its electrocatalytic activity (Figure 1b). The CVs were measured in a 0.1 M TBAP/*N*-methylpyrrolidone (NMP) solution. In the measurements under CO_2, NMP was used as a solvent instead of *o*-DCB because of the low solubility of proton source, H_2O,[14] which is essential for the catalysis,[4c] in *o*-DCB. Note that *N*,*N*-dimethylformamide (DMF), a common solvent for iron-porphyrin systems, could not be used because of the low solubility of

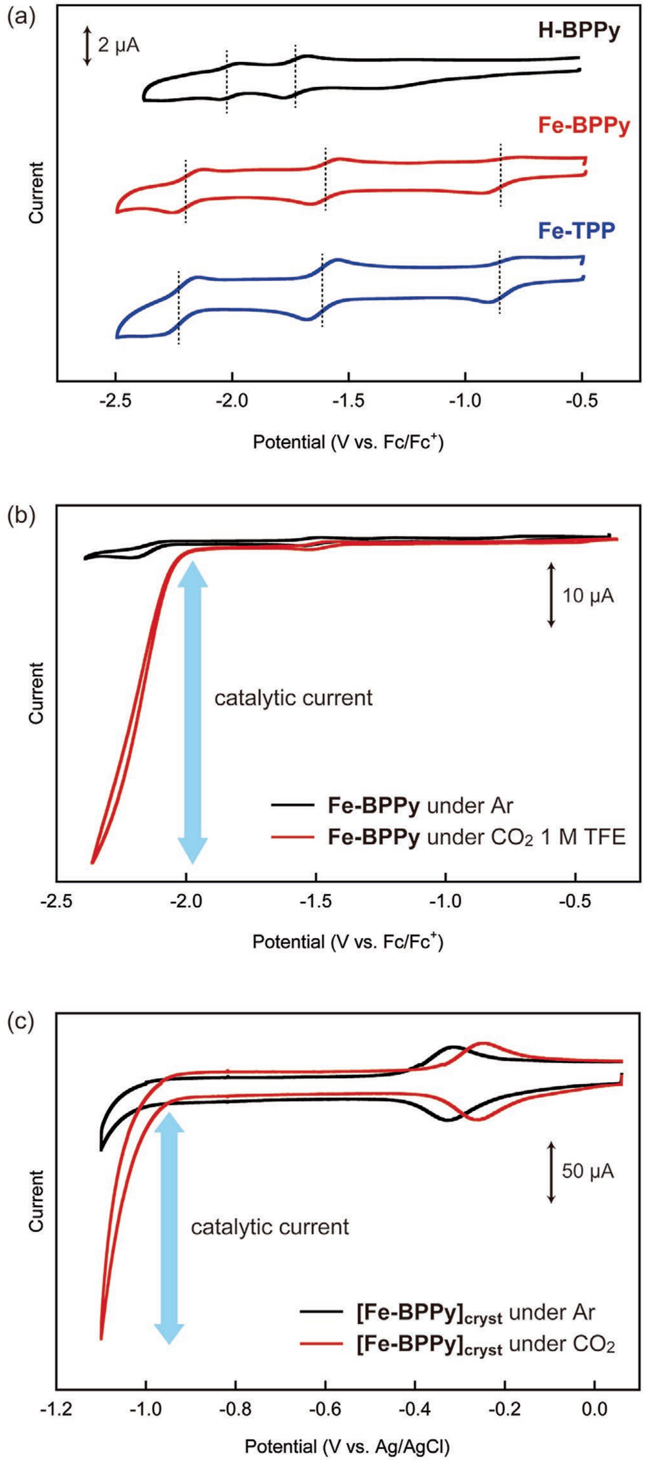

Figure 1. a) CVs of **H-BPPy**, **Fe-BPPy**, and **Fe-TPP** in 0.1 M TBAP/*o*-DCB under Ar atmosphere (WE: GC; CE: Pt wire; RE: Ag/Ag$^+$; scan rate: 100 mV s^{-1}). b) CVs of **Fe-BPPy** (0.3×10^{-3} M) in a 0.1 M TBAP/NMP solution under Ar atmosphere (blue line) and CO_2 atmosphere with 1 M TFE (red line) (WE: GC; CE: Pt wire; RE: Ag/Ag$^+$; scan rate: 20 mV s^{-1}). c) CVs of **[Fe-BPPy]$_{cryst}$** in 0.5 M $NaHCO_3$ aqueous solution under Ar atmosphere (black line) and CO_2 atmosphere (red line) (WE: carbon cloth with predeposited crystals of **[Fe-BPPy]$_{cryst}$**; CE: Pt wire; RE: Ag/AgCl (sat. KCl); scan rate: 20 mV s^{-1}).

Fe-BPPy in DMF. In the CVs of **Fe-BPPy** under Ar atmosphere, three reversible reduction peaks, which are assigned to the Fe(III)/Fe(II), Fe(II)/Fe(I), and Fe(I)/Fe(0) redox couples, were observed and are similar to the results obtained in a 0.1 м TBAP/*o*-DCB solution. When the measurement was performed under a CO_2 atmosphere with added trifluoroethanol (TFE) as a proton source, a large increase in the irreversible current was observed at the potential close to the third redox wave. The results indicate that **Fe-BPPy** can catalyze electrochemical CO_2 reduction. The similar experiments were also performed for **Fe-TPP**, and a catalytic current at similar potential and with similar intensity was observed (Figure S6, Supporting Information). This observation implies that the electrocatalytic activity two iron porphyrin complexes, **Fe-BPPy** and **Fe-TPP**, are almost identical in homogeneous state.

To further confirm the origin of the irreversible current, controlled potential electrolysis (CPE) of **Fe-BPPy** was conducted. A 0.1 м TBAP/NMP solution containing 0.3×10^{-3} м **Fe-BPPy** and 1 м TFE was electrolyzed at −2.14 V (vs Fc/Fc^+) under a CO_2 atmosphere for 1 h (for details of the CPE experiment; see also Pages S20 and S21 in the Supporting Information). After electrolysis, both gas and liquid phases were analyzed by gas chromatography and liquid phase chromatography, respectively, and CO as a major product and a small amount of formic acid as a minor product were detected (Table S3, Supporting Information). The formation of dihydrogen (H_2) was hardly detected. The faradaic efficiency (F.E.) for the conversion of CO_2 to CO was 65.9%. Note that the formation of CO was not detected in the absence of **Fe-BPPy**. These results clearly indicate that the irreversible current corresponds to electrocatalytic CO_2 reduction by **Fe-BPPy**. We also performed CPE of **Fe-TPP** under identical conditions, and the formation of CO with similar faradaic efficiency was confirmed (Table S3, Supporting Information). In both cases, the formation of HCOOH as a minor product was confirmed, although no other products, including H_2 and highly reduced products of CO_2 (i.e., HCHO, CH_3OH, and CH_4), were detected. We also determined the TOF values of CO production for **Fe-BPPy** and **Fe-TPP** based on the results of the CPE experiments (see Pages S17–S19 in the Supporting Information for details), and the TOF values were determined to be 369 (**Fe-BPPy**) and 576 s^{-1} (**Fe-TPP**). As these values are comparable, it is suggested that catalytic activity of **Fe-BPPy** and **Fe-TPP** are similar in homogeneous state. Collectively, the electronic structure and the catalytic activity of **Fe-BPPy** and **Fe-TPP** can be regarded as almost identical in homogeneous solution states.

Encouraged by the aforementioned results, we then explored the development of porous crystalline solids that serve as electrocatalysts for CO_2 reduction via the self-assembly of **Fe-BPPy**. To an *o*-DCB solution of **Fe-BPPy**, acetonitrile was slowly diffused by the liquid diffusion method, and crystalline materials suitable for single-crystal X-ray structural analysis were obtained. An Oak Ridge Thermal Ellipsoid Program (ORTEP) drawing and a summary of the crystallographic data of the obtained crystal are shown in **Figure 2**a and Table S6 in the Supporting Information, respectively. The crystal contains **Fe-BPPy**, which has an iron-porphyrin center with four peripheral pyrenylphenyl moieties at the *meso*-positions of the porphyrin ring. The packing structure of the obtained crystal is shown in Figure 2a–d. In this structure, the 1D column stabilized by head-to-head CH–π interactions between pyrenyl moieties was observed along the *a* axis. In this structure, the distances between iron centers are relatively short (5.92 and 6.21 Å; see Figure 2b for details), which is expected to serve as adjacent active centers suitable to activate CO_2 molecules.[15] As previously reported by Naruta and co-workers, by using the two iron centers with appropriate distance, the holding of CO_2 molecules can be facilitated.[15] Furthermore, such iron centers can provide a local push–pull mechanism where one iron ion acts as a Lewis base to push an electron pair to the coordinated CO_2 molecule and another iron ion acts as a Lewis acid to promote C—O bond cleavage leading to the formation of CO.[15] These 1D columns were further assembled via head-to-tail CH–π interactions (Figure 2c), which resulted in the formation of a porous framework structure (**[Fe-BPPy]**$_{\text{cryst}}$; Figure 2d). In this structure, *t*-butyl groups assist the pyrene moieties to interact with each other by filling the space close to the porphyrin ring. The size of the pore entrance in **[Fe-BPPy]**$_{\text{cryst}}$ was estimated to be 9.60×10.39 Å^2 by considering the van der Waals radii of the constituent atoms. The pores in **[Fe-BPPy]**$_{\text{cryst}}$ are surrounded by hydrophobic aromatic rings of pyrenylphenyl moieties and are large enough to accumulate small gaseous molecules. Therefore, it is expected that the pores in this porous crystalline solid can function as space to accumulate CO_2 molecules. We also examined the self-assembly of **Fe-TPP** and determined its crystal structure (**[Fe-TPP]**$_{\text{cryst}}$). The crystallographic data for **[Fe-TPP]**$_{\text{cryst}}$ are summarized in Figure S12 and Table S7 in the Supporting Information, and the packing structures are shown in Figure S13 in the Supporting Information. Unlike **[Fe-BPPy]**$_{\text{cryst}}$, **[Fe-TPP]**$_{\text{cryst}}$ has a closely packed structure without adjacent catalytic centers and pores due to the small peripheral substituents installed at the *meso*-positions of the porphyrin ring. To further clarify the porosity of **[Fe-BPPy]**$_{\text{cryst}}$ and **[Fe-TPP]**$_{\text{cryst}}$, gas adsorption studies were then conducted. **[Fe-BPPy]**$_{\text{cryst}}$ shows uptake for gases, N_2 and CO_2 at 77 and 195 K, respectively (Figure S14, Supporting Information), indicating its porous nature and ability to accumulate CO_2 gas into its pores. In contrast, **[Fe-TPP]**$_{\text{cryst}}$ exhibited negligible uptake for both N_2 and CO_2 (Figure S14, Supporting Information) because of its nonporous structure. These results clearly demonstrate that noncovalent intermolecular interactions between bulky spacers of **Fe-BPPy** provide the framework structure, **[Fe-TPP]**$_{\text{cryst}}$, which has advantageous features for CO_2 reduction aqueous media; 1) adjacent catalytic centers suitable for the activation of CO_2 molecules, and 2) hydrophobic pores suitable for the accumulation of CO_2 molecules.

The catalytic activity of this porous crystalline solid, **[Fe-BPPy]**$_{\text{cryst}}$, for CO_2 reduction under electrochemical conditions in aqueous media was then investigated. The CVs of **[Fe-BPPy]**$_{\text{cryst}}$ are shown in Figure 1c. The measurements were performed using the carbon cloth with predeposited crystals of **[Fe-BPPy]**$_{\text{cryst}}$ as a working electrode (for the details of the preparation of the electrode; see Page S30 in the Supporting Information). As a reference electrode, Ag/AgCl was used instead of Ag/Ag^+ because Ag/AgCl is a more suitable reference electrode for electrochemical measurements in aqueous media. In the CV under Ar atmosphere in 0.5 м $NaHCO_3$ aqueous solution, a reversible redox peak was observed at −0.35 V (vs Ag/AgCl; Figure 1c, black line; see Page S31 in the Supporting

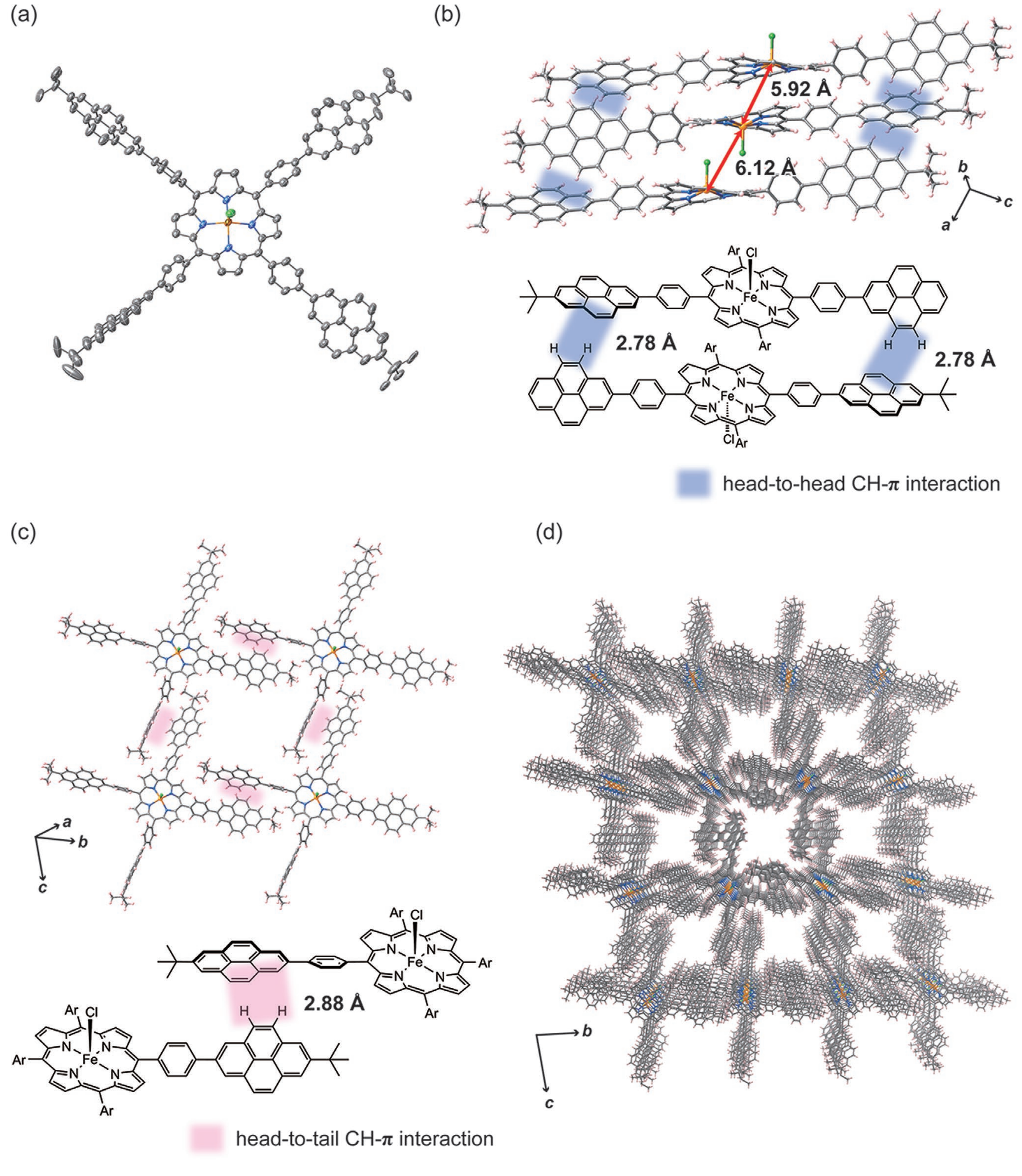

Figure 2. a) An ORTEP drawing of **Fe-BPPy** (50% probability ellipsoids). Hydrogen atoms and disordered atoms are omitted for clarity. C = gray, N = blue, Cl = green, and Fe = orange. b) 1D columnar structure observed in **[Fe-BPPy]**$_{\text{cryst}}$. c) Intercolumnar interactions observed in **[Fe-BPPy]**$_{\text{cryst}}$. d) Packing structure of **[Fe-BPPy]**$_{\text{cryst}}$ along the *a* axis.

Information for the details of interpretation of the CV). Under a CO_2 atmosphere, an increase in the irreversible current was observed at ≈–0.95 V (Figure 1c, red line), indicating the electrocatalytic activity of **[Fe-BPPy]**$_{\text{cryst}}$ in aqueous media. To quantify the product of the electrocatalysis, the CPE of **[Fe-BPPy]**$_{\text{cryst}}$ was performed. Similar to the cyclic voltammetry measurements, a carbon cloth with a predeposited complex was used as the working electrode, and electrolysis was conducted under CO_2 at –1.2 V (vs Ag/AgCl) for 1 h in 0.5 м $NaHCO_3$ aqueous solution (for details of the CPE experiment; see Pages S33 and S34 in the Supporting Information). After electrolysis, both the gas and liquid phases were analyzed. As a result, CO was a major product, and small amounts of formic acid and H_2 were detected as minor products (Figure S18 and Table S8, Supporting Information). Note that the formation of other products was not detected, although total faradaic efficiency for the production of CO, formic acid, and H_2 was 75.9%. The selectivity for CO production reached 89%, even in aqueous media. The F.E. for the conversion of CO_2 to CO was determined to be 67.5%, and the turnover number (TON) was determined to be 14.5. In addition, to ascertain that CO originated from CO_2 reduction, isotope labeling experiments were performed. We carried out CPE of **[Fe-BPPy]**$_{\text{cryst}}$ both in a) a $NaH^{13}CO_3$ aqueous solution under a $^{13}CO_2$ atmosphere and in b) a $NaH^{12}CO_3$ aqueous solution under a $^{12}CO_2$ atmosphere. Note that the use of same isotope C both for CO_2 and $NaHCO_3$ is essential because there exists equilibrium between CO_2 and bicarbonate anion (HCO_3^-). Under condition (a), 94% of ^{13}CO was produced (**Figure 3**a), as determined by mass spectrometry, whereas near-quantitative formation of ^{12}CO was confirmed under condition (b) (Figure 3b). These results clearly indicate that CO originated from CO_2 in the catalysis mediated by **[Fe-BPPy]**$_{\text{cryst}}$. The stability of **[Fe-BPPy]**$_{\text{cryst}}$ during the electrolysis was explored by scanning electron microscopy (SEM) measurements. Figures S20 and S21 in the Supporting Information show the SEM images of the crystals deposited on the carbon cloth before and after the electrolysis. The morphology of the crystals was maintained even after the electrolysis, suggesting the high stability of the system.

To clarify the effect of the porous crystalline structure of **[Fe-BPPy]**$_{\text{cryst}}$, we also investigated the catalytic activity of **Fe-TPP** in the heterogeneous state. Note that the crystalline state of **Fe-TPP** (**[Fe-TPP]**$_{\text{cryst}}$) did not exhibit a porous structure, as evidenced by single-crystal X-ray structural analysis and gas adsorption experiments (vide supra). In this experiment, **Fe-TPP** (**[Fe-TPP]**$_{\text{cryst}}$) was deposited on a carbon cloth, and CPE in aqueous media under a CO_2 atmosphere was performed. It should be also noted that the surface-active concentrations were almost identical between **[Fe-BPPy]**$_{\text{cryst}}$ and **[Fe-TPP]**$_{\text{cryst}}$ as evidenced by cyclic voltammetry (Figure S16, Supporting Information). After 1 h of electrolysis at –1.2 V (vs Ag/AgCl) in 0.5 м $NaHCO_3$ aqueous solution, both gaseous and liquid products were quantified. As a result, the formation of CO, formic acid, and H_2 was confirmed. The F.E. value for the conversion of CO_2 to CO, TON, and selectivity for CO production were determined to be 40.9%, 5.0, and 79%, respectively (Table S6, Supporting Information). These values are substantially lower than those of (**[Fe-BPPy]**$_{\text{cryst}}$ (F.E.: 67.5%, TON: 14.5, and selectivity: 89%), which clearly demonstrates that **[Fe-BPPy]**$_{\text{cryst}}$ has superior activity compared to **[Fe-TPP]**$_{\text{cryst}}$ for electrocatalytic CO_2 reduction in aqueous media. Similar to **[Fe-BPPy]**$_{\text{cryst}}$, the formation of products other than CO, formic acid, H_2 was not confirmed. As evidenced by UV–vis absorption spectroscopy and electrochemical measurements, the electronic structures of **Fe-BPPy** and **Fe-TPP** are almost identical (vide supra). Note also that the catalytic activities of these iron porphyrins are quite similar under homogeneous conditions (vide supra). In contrast, the results of the CPE experiments in a heterogeneous system revealed that the electrocatalytic performance of **[Fe-BPPy]**$_{\text{cryst}}$ is much higher than that of **[Fe-TPP]**$_{\text{cryst}}$.

To further explore the effect of structure of **[Fe-BPPy]**$_{\text{cryst}}$ on catalytic activity, cyclic voltammetry of **[Fe-BPPy]**$_{\text{cryst}}$ in D_2O was also performed. As shown in Figure S22 in the Supporting Information, the catalytic current was largely suppressed when measurement was performed in D_2O, indicating that the rate-limiting step of the reaction involves the transfer of proton. It should be noted that kinetic isotope effect (KIE) could not precisely be determined because electrolyte, $NaHCO_3$ is not deuterated. However, we have roughly estimated the KIE

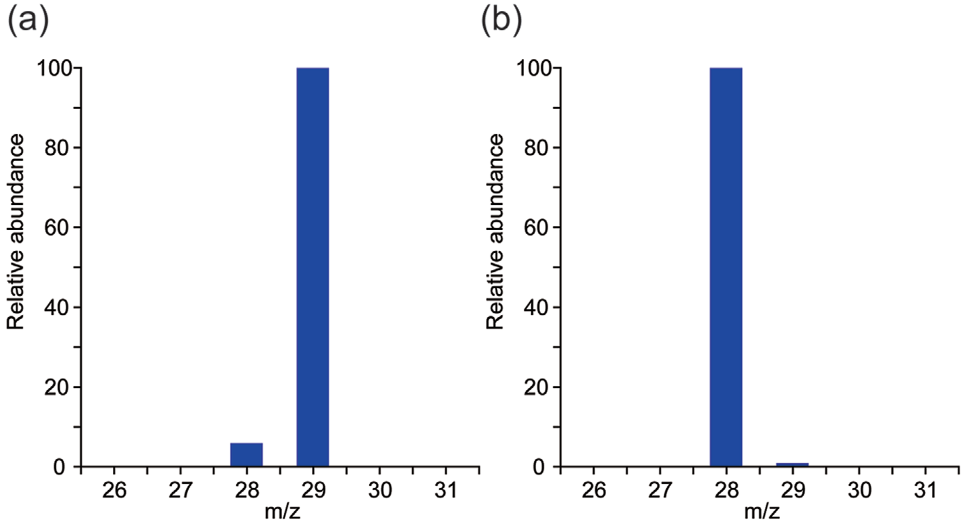

Figure 3. Mass spectra of CO generated after the CPE of **[Fe-BPPy]**$_{\text{cryst}}$ a) under $^{13}CO_2$ using a $NaH^{13}CO_3$ aqueous solution and b) under $^{12}CO_2$ using a $NaH^{12}CO_3$ aqueous solution.

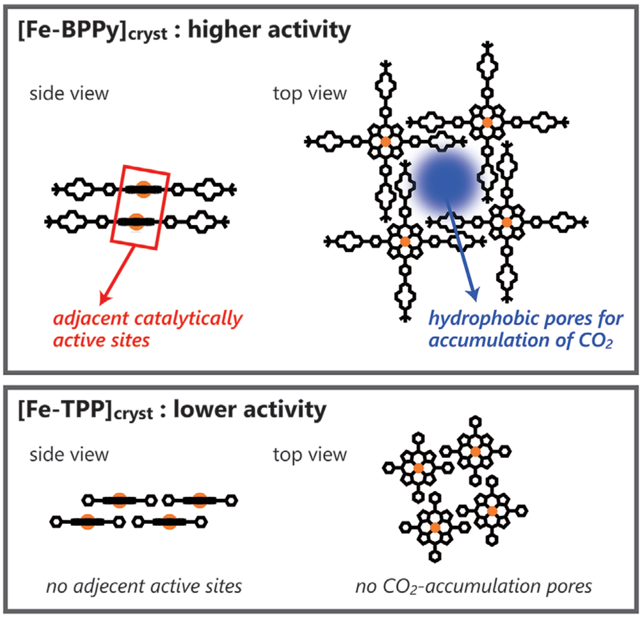

Scheme 3. Schematic illustration to summarize the features of **[Fe-BPPy]**$_{\text{cryst}}$ and **[Fe-TPP]**$_{\text{cryst}}$.

value assuming that the contribution of proton from $NaHCO_3$ is negligible, and the value was estimated to be 95 (for details of the determination of KIE value, see Pages S38 and S39 in the Supporting Information). This large KIE value strongly indicate that the rate-determining step involves the transfer of proton. This observation suggests that hydrophobic cavity efficiently accumulate CO_2 and the adjacent metal centers facilitate the coordination of CO_2 to the metal centers, and thus these processes are accelerated not to be the rate-determining step. Additionally, we have analyzed the electrochemical properties of **[Fe-BPPy]**$_{\text{cryst}}$ and **[Fe-TPP]**$_{\text{cryst}}$ by Tafel plots. In general, if a Tafel slope is close to 59 mV dec^{-1}, fast electron transfer to CO_2 occurs and the following chemical process should be a rate-determining step, while one electron reduction of CO_2 should be a rate-determining step when a Tafel slope is close to 118 mV dec^{-1}.[16] In our experiment, **[Fe-BPPy]**$_{\text{cryst}}$ exhibited a Tafel slope relatively close to 59 mV dec^{-1}, whereas the Tafel slope of **[Fe-TPP]**$_{\text{cryst}}$ were close to 118 mV dec^{-1} (for details, see Page S40 in the Supporting Information). We also performed the electrochemical impedance spectroscopy (EIS) measurements of **[Fe-BPPy]**$_{\text{cryst}}$ and **[Fe-TPP]**$_{\text{cryst}}$ under CO_2 atmosphere. From the results of EIS measurements, it was revealed that **[Fe-BPPy]**$_{\text{cryst}}$ has smaller charge transfer resistance compared to **[Fe-TPP]**$_{\text{cryst}}$, indicating that electron transfer process more easily occur in **[Fe-BPPy]**$_{\text{cryst}}$ than **[Fe-TPP]**$_{\text{cryst}}$ (for details, see Pages S41 and S42 in the Supporting Information). The results of Tafel plot and EIS measurements indicate that the **[Fe-BPPy]**$_{\text{cryst}}$ and **[Fe-TPP]**$_{\text{cryst}}$ undergo different CO_2 reduction mechanism; rate-determining step of CO_2 reduction mediated by **[Fe-BPPy]**$_{\text{cryst}}$ is a chemical process, whereas that of **[Fe-TPP]**$_{\text{cryst}}$ involves electron transfer. These facts clarify the importance of porous crystalline structures with adjacent catalytic centers and hydrophobic pores for achieving electrocatalytic CO_2 reduction in aqueous media (**Scheme 3**).

3. Conclusion

A novel highly symmetric iron-porphyrin complex with pyrene-based peripheral noncovalent interaction sites (**Fe-BPPy**) has been newly designed and synthesized. **Fe-BPPy** was easily self-assembled at room temperature via noncovalent CH–π interactions between pyrenyl moieties, and a porous crystalline framework, **[Fe-BPPy]**$_{\text{cryst}}$, formed. This **[Fe-BPPy]**$_{\text{cryst}}$ exhibited the following characteristic features: a) adjacent catalytically active sites and b) pores surrounded by hydrophobic aromatic rings. As **[Fe-BPPy]**$_{\text{cryst}}$ can be disassembled to **Fe-BPPy** in organic media, the catalytic activity of **[Fe-BPPy]**$_{\text{cryst}}$ and **Fe-BPPy** was investigated under electrochemical conditions and was compared to that of the relevant iron-porphyrin complex (**[Fe-TPP]**$_{\text{cryst}}$ and **Fe-TPP**). The electrochemical studies of **Fe-BPPy** and **Fe-TPP** in organic solvent revealed that the electronic structures and catalytic activities of these porphyrins are almost identical under homogeneous conditions. In contrast, the investigation of the catalytic activity of **[Fe-BPPy]**$_{\text{cryst}}$ and **[Fe-TPP]**$_{\text{cryst}}$ in aqueous media demonstrated that **[Fe-BPPy]**$_{\text{cryst}}$ can catalyze electrochemical CO_2 reduction with higher performance than **[Fe-TPP]**$_{\text{cryst}}$ in terms of F.E., TON, and selectivity for CO production. Given that the catalytic activities of **Fe-BPPy** and **Fe-TPP** in organic solvents (i.e., homogeneous conditions) are quite similar, the differences in catalytic activity observed in **[Fe-BPPy]**$_{\text{cryst}}$ and **[Fe-TPP]**$_{\text{cryst}}$ are concluded to arise from their difference in the packing structure. In other words, the porous crystalline nature of **[Fe-BPPy]**$_{\text{cryst}}$ with adjacent catalytically active sites is expected to be the origin of its superior activity compared to that of **[Fe-TPP]**$_{\text{cryst}}$. Collectively, the introduction of a space modulator around a catalytic center is an advantageous approach for developing porous crystalline catalysts for small-molecule conversions.

[CCDC 2033419 and 2033431 contain the supplementary crystallographic data for this paper. These data can be obtained free of charge from The Cambridge Crystallographic Data Centre via www.ccdc.cam.ac.uk/data_request/cif.]

Supporting Information

Supporting Information is available from the Wiley Online Library or from the author.

Acknowledgements

This work was supported by KAKENHI (19H02734 (R.M.), 17H06444, 19H00903, and 20K21209 (S.M.), and 15H05480, 17K19185, 17H05391, 19H04602, and 20H02754 (M.K.)) from the Japan Society for the Promotion of Science. This work was also supported by JST PRESTO (Grant Number JPMJPR20A4 (M.K.)), JST CREST (Grant Number JPMJCR20B6 (S.M.)), Research Grants in the Natural Sciences from the Mitsubishi Foundation, and the Tokuyama Science Foundation.

Conflict of Interest

The authors declare no conflict of interest.

Data Availability Statement

Research data are not shared.

Keywords

CO_2 reduction, electrocatalysis, iron porphyrin, porous crystalline solid, self-assembly

Received: October 2, 2020
Revised: February 5, 2021

---

[1] a) T. J. Meyer, *Acc. Chem. Res.* **1989**, *22*, 163; b) N. S. Lewis, D. G. Nocera, *Proc. Natl. Acad. Sci. USA* **2006**, *103*, 15729; c) A. Magnuson, M. Anderlund, O. Johansson, P. Lindblad, R. Lomoth, T. Polivka, S. Ott, K. Stensjö, S. Styring, V. Sundström, L. Hammarström, *Acc. Chem. Res.* **2009**, *42*, 1899; d) A. M. Appel, J. E. Bercaw, A. B. Bocarsly, H. Dobbek, D. L. DuBois, M. Dupuis, J. G. Ferry, E. Fujita, R. Hille, P. J. A. Kenis, C. A. Kerfeld, R. H. Morris, C. H. F. Peden, A. R. Portis, S. W. Ragsdale, T. B. Rauchfuss, J. N. H. Reek, L. C. Seefeldt, R. K. Thauer, G. L. Waldrop, *Chem. Rev.* **2013**, *113*, 6621.

[2] a) W. Leitner, *Angew. Chem., Int. Ed.* **1995**, *34*, 2207; b) X. Yin, J. R. Moss, *Coord. Chem. Rev.* **1999**, *181*, 27; c) M. R. DuBois, D. L. DuBois, *Acc. Chem. Res.* **2009**, *42*, 1974; d) M. Mikkelsen, M. Jørgensen, F. C. Krebs, *Energy Environ. Sci.* **2010**, *3*, 43; e) A. Goeppert, M. Czaun, J.-P. Jones, G. K. Surya Prakash, G. A. Olah, *Chem. Soc. Rev.* **2014**, *43*, 7995.

[3] a) K. Tanaka, D. Ooyama, *Coord. Chem. Rev.* **2002**, *226*, 211; b) J.-M. Savéant, *Chem. Rev.* **2008**, *108*, 2348; c) H. Takeda, O. Ishitani, *Coord. Chem. Rev.* **2010**, *254*, 346; d) J. Schneider, H. Jia, J. T. Muckermana, E. Fujita, *Chem. Soc. Rev.* **2012**, *41*, 2036; e) C. D. Windle, R. N. Perutz, *Coord. Chem. Rev.* **2012**, *256*, 2562; f) S. Berardi, S. Drouet, L. Francàs, C. Gimbert-Suriñach, M. Guttentag, C. Richmond, T. Stoll, A. Llobet, *Chem. Soc. Rev.* **2014**, *43*, 7501; g) T. Zhang, W. Lin, *Chem. Soc. Rev.* **2014**, *43*, 5982; h) N. Elgrishi, M. B. Chambers, X. Wang, M. Fontecave, *Chem. Soc. Rev.* **2017**, *46*, 761; i) H. Takeda, C. Cometto, O. Ishitani, M. Robert, *ACS Catal.* **2017**, *7*, 70; j) C. S. Diercks, Y. Liu, K. E. Cordova, O. M. Yaghi, *Nat. Mater.* **2018**, *17*, 301; k) J.-W. Wang, D.-C. Zhong, T.-B. Lu, *Coord. Chem. Rev.* **2018**, *377*, 225; l) B. Zhang, L. Sun, *Chem. Soc. Rev.* **2019**, *48*, 2216; m) K. E. Dalle, J. Warnan, J. J. Leung, B. Reuillard, I. S. Karmel, E. Reisner, *Chem. Rev.* **2019**, *119*, 2752; n) Q. Wang, Y. Zhang, H. Lin, J. Zhu, *Chem. - Eur. J.* **2019**, *25*, 14026.

[4] a) J. Hawecker, J.-M. Lehn, R. Ziessel, *J. Chem. Soc., Chem. Commun.* **1983**, 536; b) H. Takeda, K. Koike, H. Inoue, O. Ishitani, *J. Am. Chem. Soc.* **2008**, *130*, 2023; c) C. Costentin, S. Drouet, M. Robert, J.-M. Savéant, *Science* **2012**, *338*, 90; d) L. Chen, Z. Guo, X. -G. Wei, C. Gallenkamp, J. Bonin, E. Anxolabéhère-Mallart, K. -C. Lau, T. -C. Lau, M. Robert, *J. Am. Chem. Soc.* **2015**, *137*, 10918; e) N. Kornienko, Y. Zhao, C. S. Kley, C. Zhu, D. Kim, S. Lin, C. J. Chang, O. M. Yaghi, P. Yang, *J. Am. Chem. Soc.* **2015**, *137*, 14129; f) S. Lin, C. S. Diercks, Y.-B. Zhang, N. Kornienko, E. M. Nichols, Y. Zhao, A. R. Paris, D. Kim, P. Yang, O. M. Yaghi, C. J. Chang, *Science* **2015**, *349*, 1208; g) C. W. Machan, M. D. Sampson, C. P. Kubiak, *J. Am. Chem. Soc.* **2015**, *137*, 8564; h) H. Rao, L. C. Schmidt, J. Bonin, M. Robert, *Nature* **2017**, *548*, 74; i) T. Ouyang, H.-H. Huang, J.-W. Wang, D.-C. Zhong, T.-B. Lu, *Angew. Chem., Int. Ed.* **2017**, *56*, 738; j) C. S. Diercks, S. Lin, N. Kornienko, E. A. Kapustin, E. M. Nichols, C. Zhu, Y. Zhao, C. J. Chang, O. M. Yaghi, *J. Am. Chem. Soc.* **2018**, *140*, 1116; k) T. Ouyang, H.-J. Wang, H.-H. Huang, J.-W. Wang, S. Guo, W.-J. Liu, D.-C. Zhong, T.-B. Lu, *Angew. Chem., Int. Ed.* **2018**, *57*, 16480; l) S. K. Lee, M. Kondo, M. Okamura, T. Enomoto, G. Nakamura, S. Masaoka, *J. Am. Chem. Soc.* **2018**, *140*, 16899; m) R. Matheu, E. Gutierrez-Puebla, M. Á. Monge, C. S. Diercks, J. Kang, M. S. Prévot, X. Pei, N. Hanikel, B. Zhang, P. Yang, O. M. Yaghi, *J. Am. Chem. Soc.* **2019**, *141*, 17081; n) X. Feng, Y. Pi, Y. Song, C. Brzezinski, Z. Xu, Z. Li, W. Lin, *J. Am. Chem. Soc.* **2020**, *142*, 690.

[5] a) A. J. Morria, G. J. Meyer, E. Fujita, *Acc. Chem. Res.* **2009**, *42*, 1983; b) C. Costentin, M. Robert, J.-M. Savéant, *Chem. Soc. Rev.* **2013**, *42*, 2423; c) C. Costentin, M. Robert, J.-M. Savéant, *Acc. Chem. Res.* **2015**, *48*, 2996.

[6] a) C. Costentin, G. Passard, M. Robert, J.-M. Savéant, *Proc. Natl. Acad. Sci. USA* **2014**, *111*, 14990; b) R. B. Ambre, Q. Daniel, T. Fan, H. Chen, B. Zhang, L. Wang, M. S. G. Ahlquist, L. Duan, L. Sun, *Chem. Commun.* **2016**, *52*, 14478; c) Y. Okabe, S. K. Lee, M. Kondo, S. Masaoka, *J. Biol. Inorg. Chem.* **2017**, *22*, 713.

[7] a) B. Wang, R.-B. Lin, Z. Zhang, S. Xiang, B. Chen, *J. Am. Chem. Soc.* **2020**, *142*, 14399; b) I. Hisaki, X. Chen, K. Takahashi, T. Nakamura, *Angew. Chem., Int. Ed.* **2019**, *58*, 11160.

[8] a) D. P. Lydon, P. Li, A. C. Benniston, W. McFarlane, R. W. Harrington, W. Clegg, *Eur. J. Org. Chem.* **2007**, *10*, 1653; b) B. B. Shrestha, S. Higashibayashi, H. Sakurai, *Beilstein J. Org. Chem.* **2014**, *10*, 841; c) M. A. Dobrowolski, G. Garbarino, M. Mezouar, A. Ciesielski, M. K. Cyrański, *CrystEngComm* **2014**, *16*, 415; d) A. Nagai, Y. Okabe, *Chem. Commun.* **2014**, *50*, 10052.

[9] a) A. Stockmann, J. Kurzawa, N. Fritz, N. Acar, S. Schneider, J. Daub, R. Engl, T. Clark, *J. Phys. Chem. A* **2002**, *106*, 7958; b) M. Raytchev, E. Pandurski, I. Buchvarov, C. Modrakowski, T. Fiebig, *J. Phys. Chem. A* **2003**, *107*, 4592; c) W. Weigel, W. Rwttig, M. Dekhtyar, C. Modrakowski, M. Beinhoff, A. D. Schlüter, *J. Phys. Chem. A* **2003**, *107*, 5941; d) W. Wu, W. Wu, S. Ji, H. Guo, X. Wang, J. Zhao, *Dyes Pigm.* **2011**, *89*, 199.

[10] M. Gouterman, *J. Chem. Phys.* **1959**, *30*, 1139.

[11] M. Gouterman, *J. Mol. Spectrosc.* **1961**, *6*, 138.

[12] T. Dhanasekaran, J. Grodkowski, P. Neta, P. Hambright, E. Fujita, *J. Phys. Chem. A* **1999**, *103*, 7742.

[13] M. Hammouche, D. Lexa, J.-M. Savéant, M. Momenteau, *J. Electroanal. Chem. Interfacial Electrochem.* **1988**, *249*, 347.

[14] a) C. Costentin, S. Drouet, G. Passard, M. Robert, J.-M. Savéant, *J. Am. Chem. Soc.* **2013**, *135*, 9023; b) A. Fukatsu, M. Kondo, Y. Okabe, S. Masaoka, *J. Photochem. Photobiol., A* **2015**, *313*, 143.

[15] E. A. Mohamed, Z. N. Zahran, Y. Naruta, *Chem. Commun.* **2015**, *51*, 16900.

[16] a) S. Gao, X. Jiao, Z. Sun, W. Zhang, Y. Sun, C. Wang, Q. Hu, X. Zu, F. Yang, S. Yang, L. Liang, J. Wu, Y. Xie, *Angew. Chem., Int. Ed.* **2016**, *55*, 698; b) C. W. Lee, N. H. Cho, S. W. Im, M. S. Jee, Y. J. Hwang, B. K. Min, K. T. Nam, *J. Mater. Chem. A* **2018**, *6*, 14043.